

On Oversampling-Based Signal Detection

A pragmatic approach

Andrea Mariani · Andrea Giorgetti · Marco Chiani

Received: 31 January 2019 / Revised: 14 June 2019 / Accepted: 6 July 2019

Abstract The availability of inexpensive devices allows nowadays to implement cognitive radio (CR) functionalities in large-scale networks such as the internet-of-things (IoT) and future mobile cellular systems. In this paper, we focus on wideband spectrum sensing (WSS) in the presence of oversampling, i.e., the sampling frequency of a digital receiver is larger than the signal bandwidth, where signal detection must take into account the front-end impairments of low-cost devices. Based on the noise model of a software-defined radio (SDR) dongle, we address the problem of robust signal detection in the presence of noise power uncertainty and non-flat noise power spectral density (PSD). In particular, we analyze the receiver operating characteristic (ROC) of several detectors in the presence of such front-end impairments, to assess the performance attainable in a real-world scenario. We propose new frequency-domain detectors, some of which are proven to outperform previously proposed spectrum sensing techniques such as, e.g., eigenvalue-based tests. The

study shows that the best performance is provided by a noise-uncertainty immune energy detector (ED) and, for the colored noise case, by tests that match the PSD of the receiver noise.

Keywords Cognitive radio · colored noise · detection · Internet-of-Things · noise uncertainty · oversampling · wideband spectrum sensing

1 Introduction

The increasing demand for a limited resource such as the radio-frequency (RF) spectrum is the propelling force toward new ways radio ecosystems can coexist. For example, the coexistence between radar and wireless communications is a topic which recently received increasing attention by the DARPA and the US National Spectrum Consortium [1, 2]. To this aim, cognitive radio (CR) systems represent a paradigm to opportunistically access the spectrum provided that the RF environment is monitored through the so-called spectrum sensing (SS) [3, 4]. The objective of SS is to infer the presence of signals in a frequency band, thus identifying spectrum holes and enabling primary user (PU) protection.

Software-defined radio (SDR) was born with the aim of building flexible front-ends for transceivers in which radio functionalities are controlled and programmable by software [5–8]. In the last decade, SDR gained a renewed interest for implementing multi-band multi-standard platforms, in particular to enable CR [6–11]. In parallel, we have seen the development and diffusion of several general purpose high-performance SDRs such as universal software radio platforms (USRPs) [12]. However, in the context of internet-of-things (IoT) low-cost low-complexity SDRs appear more appropriate. There

This work was supported in part by MIUR under the program “Dipartimenti di Eccellenza (2018-2022) - Precise-CPS,” and in part by the EU project eCircular (EIT Climate-KIC). The material in this paper was presented in part at the IEEE Int. Symp. on Personal, Indoor and Mobile Radio Comm. (PIMRC 2018), Bologna, Italy, Sep. 2018.

A. Mariani
Onit Group S.r.l.
Via dell’Arrigoni 308, 47522 Cesena (FC), Italy
E-mail: amariani@onit.it

A. Giorgetti and M. Chiani
CNIT, IEIIT/CNR, Dept. of Electrical, Electronic, and Information Engineering “Guglielmo Marconi” (DEI)
University of Bologna
Via dell’Università 50, 47522 Cesena (FC), Italy
E-mail: andrea.giorgetti@unibo.it
E-mail: marco.chiani@unibo.it

are several examples of such SDRs that can be used for SS and, among them, one very popular is represented by the digital video broadcasting–terrestrial (DVB-T) dongle based on the Realtek RTL2832U chipset.

The adoption of low-cost devices is, on the other hand, critical for wideband spectrum sensing (WSS) due to the presence of receiver nonidealities which have a substantial impact on detection performance, especially at very low signal-to-noise ratios (SNRs) [13, 14]: colored noise, noise power uncertainty, in-phase and quadrature-phase imbalance, nonlinearities, spurs, phase noise, and aliasing [15–17]. It is therefore essential to perform a proper characterization of the receiver front-end and to design robust detection strategies.

Regarding noise, it is common to adopt the ubiquitous additive white Gaussian noise (AWGN) model [18–20]. However, wideband receivers are often affected by a non-white noise power spectral density (PSD), which corresponds to noise temporal correlation, mainly caused by filtering in the receiver chain [21]. Signal detection in colored noise is studied in [22] using classical hypothesis testing approaches, while the effect of noise correlation on some eigenvalue based algorithms is analyzed in [23].

Another impairment is represented by noise power fluctuations (caused e.g., by receiver temperature variations) often referred as noise uncertainty [19, 24, 25]. This issue can be counteracted either by adopting noise power estimation strategies [13, 19, 26] or by adopting detection metrics which are independent on the noise power. In the latter case, time-domain tests that infer the presence of correlation among the received samples have been proposed, in particular exploiting eigenvalues of the sample covariance matrix (SCM) [20, 21, 23, 27, 28]. This is also the case of sensing in the spatial domain, where the correlation among multiple antennas or sensor nodes (by cooperation), due to the presence of a common signal, is exploited [3, 21, 29, 30].

A key element of WSS is that the receiving bandwidth is larger than that of the signal-to-be-detected (StD), hence for digital receivers oversampling is often the rule [31–33]. This fact can be exploited both in the frequency-domain as well as in the time-domain. For example, since oversampling implies correlation in time, detectors based on correlation properties of the received signal are the most common [21, 23, 29, 34–36]. Another significant element is that the literature on oversampling-based detection explores the case where the StD has a known band, i.e., center frequency and bandwidth. However, in some contexts like opportunistic spectrum access, it is necessary to infer the presence of any signal in the observed frequency slot without knowing its band a priori [26, 28].

In this paper, we focus on oversampling-based signal detection in the presence of noise power uncertainty, considering both white and colored Gaussian noise. The noise model is derived from the statistical analysis of a popular SDR, suitable for low-cost, large-scale RF monitoring.

The key contributions of this paper are as follows:

- We analyze the problem of sensing the spectrum in a setting that combines the presence of colored Gaussian noise and noise power uncertainty when the sampling frequency is higher than the signal bandwidth.
- We revisit several detectors proposed in the literature, and we derive their performance in terms of receiver operating characteristic (ROC).
- We propose new detectors which outperform the existing ones in the specific setting, exhibiting robustness against front-end impairments: a frequency domain version of the energy detector (ED) with estimated noise power (ENP), a detector that measures the spectral flatness, and a spectrum correlation - based detector.
- Different scenarios are considered: i) unknown signal band; ii) known signal bandwidth but unknown center frequency; iii) both signal bandwidth and center frequency known.
- The performance is derived in the presence of a signal model extracted from the statistical characterization of the noise of a low-cost SDR receiver.

The analysis showed that the best detection performance is provided by a noise-uncertainty immune ED and, for the colored noise case, by tests that match the PSD of the receiver noise. To the best of our knowledge, WSS in this setting is underexplored.

The paper is organized as follows. In Section 2 the system model is introduced. Section 3 proposes detectors in the presence of white noise, while Section 4 analyzes detection with colored noise. A case study based on the characterization of a real SDR receiver is illustrated in Section 5, and the corresponding numerical results are presented in Section 6. Conclusions are drawn in the last section.

Throughout the paper, boldface letters denote matrices and vectors. Moreover, \mathbf{I}_m represents the $m \times m$ identity matrix, $\text{tr}\{\mathbf{A}\}$ is the trace of the matrix \mathbf{A} , $\text{diag}\{\mathbf{A}\}$ stands for a matrix which contains only the principal diagonal of the matrix \mathbf{A} , $(\cdot)^T$ and $(\cdot)^H$ stand, respectively, for simple and Hermitian transposition. The ℓ_p -norm of the vector \mathbf{v} is $\|\mathbf{v}\|_p \triangleq \sqrt[p]{\sum_i |v_i|^p}$, where v_i is the i th element of \mathbf{v} .

2 System model

The detection task is to distinguish the presence or absence of any signal in the observed band. The two hypotheses are denoted, respectively, by \mathcal{H}_1 and \mathcal{H}_0 . We consider a receiver equipped with a single antenna. After down-conversion and sampling, the N -length column vector of the received complex samples is given by

$$\mathbf{y} = \begin{cases} \mathbf{s} + \mathbf{n}, & \mathcal{H}_1 \\ \mathbf{n}, & \mathcal{H}_0 \end{cases} \quad (1)$$

where \mathbf{n} denotes noise and \mathbf{s} contains the transmitted signal samples including channel effects. Let us consider a bandlimited StD with band $\mathcal{B} = [f_L, f_H]$ and bandwidth $B = f_H - f_L$. Oversampling is implemented using a sampling rate $f_s = \text{OSF} \cdot B$, where OSF is the integer oversampling factor (OSF) [21, 35]. The SNR is defined as $\text{SNR} = \sigma_s^2 / \sigma^2$, where $\sigma_s^2 = \mathbb{E}\{\mathbf{s}^H \mathbf{s}\}$ and $\sigma^2 = \mathbb{E}\{\mathbf{n}^H \mathbf{n}\}$. Without loss of generality we assume that both \mathbf{s} and \mathbf{n} are modeled as vectors of zero mean random variables (r.v.s).

The noise power is often uncertain and varying in time. This is mainly due to effects such as temperature variations, changes in low noise amplifier gain due to thermal fluctuations, and initial calibration errors [19, 24, 25]. We express the noise samples vector as $\mathbf{n} = \sigma \tilde{\mathbf{n}}$, where $\tilde{\mathbf{n}}$ are zero mean complex Gaussian samples with unit variance, and the noise power σ^2 is an unknown time-varying parameter. However, its variations are generally slow, and thus σ^2 can be considered constant during the collection of the N samples [25].

The most common assumption in the literature is to model noise as a white Gaussian process. This is a desirable condition for every receiver, and it is a realistic model for well-designed systems. However, low-cost wideband devices generally present a colored noise PSD, which is mainly due to filtering [21–23]. A statistical description of the noise derived from samples captured by a SDR device is presented in Section 5.1. Based on such analysis, we model noise as a correlated Gaussian process.

The detection tests proposed in the next sections exploit the knowledge of the second-order statistical properties of receiver noise, although noise power remains unknown. We consider, therefore, that detection is preceded by an off-line calibration stage (under hypothesis \mathcal{H}_0), in which the system estimates either the noise PSD, $\mathcal{W}(f)$, for frequency-domain detectors, or the noise covariance matrix, Σ_0 , for time-domain detectors (see Section 5.2 for details). In both cases, due to noise uncertainty, the noise PSD and the covariance

matrix are known except for a multiplicative factor related to the time-varying noise power.¹

2.1 Frequency-domain representation: periodogram

Frequency-domain spectrum sensing is based on the estimation of a spectral representation of received samples and adoption of a test to infer the presence or absence of a signal. For simplicity, the frequency-domain representation is based on the PSD estimation through the averaged periodogram (also known as Bartlett's periodogram), by a N_{fft} -points discrete Fourier transform (DFT) [37, Section 12.2.1]. In particular, assuming that the total number of samples is $N = N_{\text{fft}} N_{\text{avg}}$, the i th element of the averaged periodogram $\mathbf{p} = (p_0, \dots, p_{N_{\text{fft}}-1})$ is computed as [37]

$$p_i = \frac{1}{N_{\text{fft}} N_{\text{avg}}} \sum_{k=1}^{N_{\text{avg}}} \left| \sum_{m=1}^{N_{\text{fft}}} y_{m+(k-1)N_{\text{fft}}} e^{-j2\pi \frac{im}{N_{\text{fft}}}} \right|^2 \quad (2)$$

where y_l is the l th element of the received vector \mathbf{y} .

The Bartlett's periodogram can be used also to estimate the noise PSD during the calibration phase. In the following, we denote with $\mathbf{w} = (w_0, \dots, w_{N_{\text{fft}}-1})$ the vector containing the estimate of the noise PSD, $\mathcal{W}(f)$, calculated as

$$w_i = \frac{1}{N_{\text{fft}} N_{\text{avg}}} \sum_{k=1}^{N_{\text{avg}}} \left| \sum_{m=1}^{N_{\text{fft}}} n_{m+(k-1)N_{\text{fft}}} e^{-j2\pi \frac{im}{N_{\text{fft}}}} \right|^2. \quad (3)$$

2.2 Time-domain representation: sample covariance

Using oversampling, time-domain tests can exploit the correlation properties of \mathbf{y} to distinguish the StD from white Gaussian noise (WGN). In fact, under \mathcal{H}_0 the covariance matrix of white noise is $\Sigma_0 = \mathbb{E}\{\mathbf{nn}^H\} = \sigma^2 \mathbf{I}_N$ and thus its eigenvalues are all equal to σ^2 . Conversely, under \mathcal{H}_1 , the eigenvalues are not all equal. Therefore, eigenvalue-based tests measure the eigenvalue spread to discriminate between \mathcal{H}_0 and \mathcal{H}_1 .

When the signal covariance $\Sigma = \mathbb{E}\{\mathbf{yy}^H\}$ is unknown, the SCM of \mathbf{y} is used instead [20, 21, 23, 27]. In this case, the detector arranges the received vector \mathbf{y} in

¹Note that although the detectors presented do not depend on the noise power, its fluctuations reflect on the SNR, which in turn have an impact on the performance of the tests. This aspect must be taken into account in the study of the decision threshold setting, which is out of the scope of the paper.

a $p \times q$ matrix (p and q are such that $N \geq pq$)

$$\mathbf{Y} = \begin{bmatrix} y_1 & y_{p+1} & \cdots & y_{(q-1)p+1} \\ y_2 & y_{p+2} & \cdots & y_{(q-1)p+2} \\ \cdots & \cdots & \cdots & \cdots \\ y_p & y_{2p} & \cdots & y_{qp} \end{bmatrix}. \quad (4)$$

Then, the eigenvalues of the SCM $\mathbf{S} = \mathbf{Y}\mathbf{Y}^H/q$, denoted as $\lambda_1 \geq \lambda_2 \geq \cdots \geq \lambda_p$, are used as estimate of the eigenvalues of $\mathbf{\Sigma}$. Previous works adopt $p = \text{OSF}$ and $q = \lfloor N/p \rfloor$ [23, 29]. In this case, the rows of \mathbf{Y} are sequences obtained using a sampling period equal to the symbol duration. Assuming the StD composed by independent symbols, if $p = \text{OSF}$ the rows of \mathbf{Y} tend to be independent, while columns are correlated.²

Alternatively, some tests are based on the sample correlation matrix obtained by normalizing the SCM as

$$\mathbf{R} = \text{diag}\{\mathbf{S}\}^{-1/2} \mathbf{S} \text{diag}\{\mathbf{S}\}^{-1/2}. \quad (5)$$

The sample correlation matrix element r_{ij} is the Pearson correlation coefficient between the columns i and j of \mathbf{Y} . In the following, we denote with $\mu_1 \geq \mu_2 \geq \cdots \geq \mu_p$ the eigenvalues of \mathbf{R} .

3 White Noise

In this section, we present WSS detectors in the presence of white Gaussian noise and noise power uncertainty.

3.1 Frequency-domain detectors

3.1.1 Energy-based detectors

The conventional implementation of the ED considers the received signal power as a test statistic. Thus, the frequency-domain version of the ED is given by³⁴

$$T_{\text{ed-all}} = \frac{\mathcal{H}_1}{\mathcal{H}_0} \geq \xi. \quad (6)$$

When the StD bandwidth is smaller than the receiver bandwidth, the test statistic $T_{\text{ed-all}}$ (6) also includes the noise-only contributions that come from samples of the PSD which are out of the signal band. It is, therefore,

²In this case the oversampling-based detection problem turns out to be equivalent to spectrum sensing with multiple antennas.

³Note that by Parseval's theorem we have $T_{\text{ed-all}} = \frac{1}{N_{\text{avg}}} \sum_i \mathbf{y}_i^H \mathbf{y}_i$, which is proportional to the usual ED metric [19].

⁴In the paper ξ denotes any detection threshold.

reasonable to modify the ED metric, including only the frequency components that may contain the signal. Denoting as $\mathbf{p}_{[\mathcal{B}]}$ the vector that contains the periodogram bins for $f_L \leq f \leq f_H$ we propose the test

$$T_{\text{ed}} = \frac{\mathcal{H}_1}{\mathcal{H}_0} \geq \xi. \quad (7)$$

Note that (6) and (7) depend on the noise power and thus may suffer noise uncertainty. To counteract this problem, schemes that compute the ENP can be adopted [19]. In the oversampling scenario, the noise power can be estimated from the noise-only bands. Thus, the frequency-domain version of the ENP-ED test is given by

$$T_{\text{enp-ed}} = \frac{\|\mathbf{p}_{[\mathcal{B}]}\|_1}{\|\mathbf{p}_{[\mathcal{B}]}\|_1} \frac{\mathcal{H}_1}{\mathcal{H}_0} \geq \xi \quad (8)$$

where $\mathbf{p}_{[\mathcal{B}]}$ is the vector containing the periodogram bins that are out of the signal band. In the Appendix, we prove that $T_{\text{enp-ed}}$ is the generalized likelihood ratio test (GLRT) when the StD is modeled as a bandlimited Gaussian random process with flat PSD within \mathcal{B} .

3.1.2 Flatness-based detectors

In the presence of white noise, some frequency-domain tests are based on the measure of the *flatness* of the received signal PSD. A flat spectrum is expected, indeed, under \mathcal{H}_0 , contrarily \mathcal{H}_1 occurs. An example is the arithmetic-geometric mean ratio test (AGM) [31]

$$T_{\text{f-agm}} = \frac{\frac{1}{N_{\text{fft}}} \sum_{i=1}^{N_{\text{fft}}} p_i}{\left(\prod_{i=1}^{N_{\text{fft}}} p_i \right)^{1/N_{\text{fft}}}} \frac{\mathcal{H}_1}{\mathcal{H}_0} \geq \xi. \quad (9)$$

Another way to measure spectrum flatness is to build a test which is the ratio between the ℓ_1 -norm and the ℓ_2 -norm of \mathbf{p} , as

$$T_{\text{sf}} = \frac{1}{\sqrt{N_{\text{fft}}}} \frac{\|\mathbf{p}\|_1}{\|\mathbf{p}\|_2} \frac{\mathcal{H}_0}{\mathcal{H}_1} \geq \xi. \quad (10)$$

The rationale behind (10) is that its inverse is similar to the population coefficient of variation (CV), a statistical parameter defined as the ratio of the sample standard deviation to the sample mean. The CV is often used in statistics and related disciplines as a measure of the variability of a series of samples. In our setting, under \mathcal{H}_0 all w_i 's are very similar because of the white PSD of noise, so we have approximatively $T_{\text{sf}} = 1$ irrespectively of the noise power. Moreover, because of

the well-known inequality $\|\mathbf{p}\|_1 \leq \sqrt{N_{\text{fft}}} \|\mathbf{p}\|_2$ we have $T_{\text{sf}} \leq 1$.

Note that $T_{\text{ed-all}}$, $T_{\text{f-agm}}$, and T_{sf} do not require the knowledge of \mathcal{B} , which instead must be known for the ED-based tests T_{ed} and $T_{\text{enp-ed}}$. Different detectors can be conceived with a partial knowledge of the StD characteristics. Considering the case in which only B is known, one can search for the band that contains the maximum received power. Thus, similarly to (8) we propose the test

$$T_{\text{search-B}} = \frac{\max_{\mathcal{C}_B} \|\mathbf{p}_{[\mathcal{C}_B]}\|_1}{\|\mathbf{p}\|_1} \underset{\mathcal{H}_0}{\overset{\mathcal{H}_1}{\geq}} \xi \quad (11)$$

where \mathcal{C}_B is any frequency slot, with bandwidth B , contained in the receiver band.

3.2 Time-domain detectors

3.2.1 Eigenvalue-based tests

Eigenvalue-based tests are probably the most popular detectors studied in the presence of white noise [20, 21, 23, 27, 29]. Of considerable importance there are the sphericity test (also called AGM) [27, 38], the maximum to minimum eigenvalues ratio (MME) [21, 23], the ratio of maximum eigenvalue to the trace (MET) [20] and the locally best invariant (LBI) test [20, 39]. The corresponding decision metrics are given by

$$\begin{aligned} T_{\text{sph}} &= \frac{(\prod_{i=1}^p \lambda_i)^{1/p}}{(\sum_{i=1}^p \lambda_i)/p} \underset{\mathcal{H}_1}{\overset{\mathcal{H}_0}{\geq}} \xi & T_{\text{mme}} &= \frac{\lambda_1}{\lambda_p} \underset{\mathcal{H}_1}{\overset{\mathcal{H}_0}{\geq}} \xi \\ T_{\text{met}} &= \frac{\lambda_1}{\sum_{i=1}^p \lambda_i} \underset{\mathcal{H}_1}{\overset{\mathcal{H}_0}{\geq}} \xi & T_{\text{lbi}} &= \frac{\sum_{i=1}^p \lambda_i^2}{(\sum_{i=1}^p \lambda_i)^2} \underset{\mathcal{H}_1}{\overset{\mathcal{H}_0}{\geq}} \xi. \end{aligned} \quad (12)$$

We also consider three tests based on the sample correlation matrix \mathbf{R} (5), namely the test of independence [27], the Frobenius norm test [40], and the maximum eigenvalue test, defined, respectively, as

$$\begin{aligned} T_{\text{ind}} &= \prod_{i=1}^p \frac{\mu_i}{\mathcal{H}_1} \underset{\mathcal{H}_1}{\overset{\mathcal{H}_0}{\geq}} \xi & T_{\text{fro}} &= \sum_{i=1}^p \mu_i^2 \underset{\mathcal{H}_1}{\overset{\mathcal{H}_0}{\geq}} \xi \\ T_{\text{max}} &= \mu_1 \underset{\mathcal{H}_1}{\overset{\mathcal{H}_0}{\geq}} \xi. \end{aligned} \quad (13)$$

All the tests defined above are independent of the noise power. We do not include in the analysis eigenvalue-based tests that suffer noise uncertainty, such as the Wilk's test [20].

3.2.2 Autocorrelation-based detectors

In this section, we discuss some alternative tests that exploit the correlation properties of \mathbf{y} , but cannot be expressed as functions of the eigenvalues of the SCM or \mathbf{R} . One of the most popular detector in this context is the covariance-based detector [41]

$$T_{\text{cov}} = \frac{\sum_{n=1}^p \sum_{m=1}^p |s_{n,m}|}{\text{tr}\{\mathbf{S}\}} \underset{\mathcal{H}_0}{\overset{\mathcal{H}_1}{\geq}} \xi. \quad (14)$$

Some modifications of this detector have been proposed in [42, 43].

In [35], autocorrelation-based approaches specifically for detection in the presence of oversampling have been discussed. In particular, two detectors proposed are

$$T_{\text{ac}} = \sum_{i=1}^{\text{OSF}-1} |\mathbf{y}_{\{i\}}^H \mathbf{y} + v_i|^2 \underset{\mathcal{H}_0}{\overset{\mathcal{H}_1}{\geq}} \xi \quad (15)$$

$$T_{\text{ac-1}} = |\mathbf{y}_{\{1\}}^H \mathbf{y} + v_1|^2 \underset{\mathcal{H}_0}{\overset{\mathcal{H}_1}{\geq}} \xi \quad (16)$$

where $\mathbf{y}_{\{i\}}$ denotes a circular shift of \mathbf{y} by i steps, $v_i = N\alpha_i\sigma_s^2 / (2\text{SNR}_{\text{ref}} + N\text{SNR}_{\text{ref}}^2 (\alpha_i^2 + 2i^2/\text{OSF}/N))$, and $\alpha_i = (\text{OSF} - i)/\text{OSF}$. The reference SNR parameter SNR_{ref} should be set equal to SNR. However, since in practice, SNR is unknown, it can be calculated as the SNR corresponding to the weakest signal power required to perform detection.

4 Colored Noise

In this section, we present WSS detectors in the presence of colored Gaussian noise and noise power uncertainty.

4.1 Frequency-domain detectors

4.1.1 Energy-based detectors

Energy-based detectors (6)-(8) can be used to infer the presence of a signal in the observed band in non-flat noise PSD case. Regarding (8), note that both the numerator and the denominator are proportional to σ^2 ; thus, such a detector does not suffer noise uncertainty.

A modification of $T_{\text{enp-ed}}$ for the colored noise case can be obtained applying *frequency-domain whitening*,

consisting of defining the vector $\mathbf{q} = (q_0, \dots, q_{N_{\text{fft}}-1})$, with elements $q_i = \frac{p_i}{w_i}$. The resulting test is

$$T_{\text{w-enp-ed}} = \frac{\|\mathbf{q}_{[\mathcal{B}]}\|_1}{\|\mathbf{q}_{[\overline{\mathcal{B}]}\|_1} \frac{\mathcal{H}_1}{\mathcal{H}_0} \geq \xi \quad (17)$$

where $\mathbf{q}_{[\mathcal{B}]}$ and $\mathbf{q}_{[\overline{\mathcal{B}]}$ are analogous of $\mathbf{p}_{[\mathcal{B}]}$ and $\mathbf{p}_{[\overline{\mathcal{B}]}$ in (8). Note that w_i are the elements of \mathbf{w} calculated during the calibration phase by (3).

4.1.2 Flatness-based detectors

Considering the AGM, after whitening, we get the test [33]

$$T_{\text{wf-agm}} = \frac{\frac{1}{N_{\text{fft}}} \sum_{i=1}^{N_{\text{fft}}} q_i}{\prod_{i=1}^{N_{\text{fft}}} q_i^{1/N_{\text{fft}}}} \frac{\mathcal{H}_1}{\mathcal{H}_0} \geq \xi. \quad (18)$$

4.1.3 Noise PSD matching detectors

Under hypothesis \mathcal{H}_0 the vector \mathbf{p} exhibits a high degree of similarity with \mathbf{w} , while they should differ under \mathcal{H}_1 . A method to measure the similarity is the degree of correlation between \mathbf{p} and \mathbf{w} , which leads to the following test

$$T_{\text{fc}} = \frac{\mathbf{p}^T \mathbf{w}}{\|\mathbf{p}\|_2 \|\mathbf{w}\|_2} \frac{\mathcal{H}_0}{\mathcal{H}_1} \geq \xi \quad (19)$$

where the decision metric is the correlation coefficient between \mathbf{p} and \mathbf{w} .

Alternatively, the Kullback-Leibler (K-L) divergence between \mathbf{p} and \mathbf{w} can be adopted as decision test. In order to avoid noise uncertainty we adopt the normalized vectors $\tilde{\mathbf{p}} = \mathbf{p}/\|\mathbf{p}\|_1$ and $\tilde{\mathbf{w}} = \mathbf{w}/\|\mathbf{w}\|_1$, and thus the detector is given by

$$T_{\text{fkl}} = \sum_{i=1}^{N_{\text{fft}}} \tilde{p}_i \log \frac{\tilde{p}_i}{\tilde{w}_i} \frac{\mathcal{H}_1}{\mathcal{H}_0} \geq \xi. \quad (20)$$

Note that both (19) and (20) are novel. In [44] a test similar to (19) without normalization is adopted when the StD spectrum is known a priori and the noise is white. On the contrary, our test assumes that noise is colored, and its PSD known from the calibration phase, while the StD spectrum is unknown.

4.2 Time-domain detectors

When noise is colored, eigenvalue-based algorithms can be adopted if *time-domain whitening* is applied to the received samples before detection [21].⁵ In this domain, whitening is based on the calibration phase described in Section 2, from which the SCM of noise under \mathcal{H}_0 , $\mathbf{S}_0 = \mathbf{Y}\mathbf{Y}^H/q$, is obtained. Eigenvalue tests can then be applied considering now the eigenvalues $\lambda_1^{\mathbf{B}} \geq \lambda_2^{\mathbf{B}} \geq \dots \geq \lambda_p^{\mathbf{B}}$ of $\mathbf{B}\mathbf{S}_0\mathbf{B}^H$, where \mathbf{B} is the whitening matrix, i.e., a matrix such that $\mathbf{B}\mathbf{S}_0\mathbf{B}^H = \mathbf{I}_p$. Therefore, the sphericity test in the presence of colored noise becomes

$$T_{\text{w-sph}} = \frac{(\prod_{i=1}^p \lambda_i^{\mathbf{B}})^{1/p} \mathcal{H}_0}{(\sum_{i=1}^p \lambda_i^{\mathbf{B}})/p \mathcal{H}_1} \geq \xi. \quad (21)$$

Similarly, considering the tests based on \mathbf{R} , we can adopt detectors based on $\mu_1^{\mathbf{K}} \geq \mu_2^{\mathbf{K}} \geq \dots \geq \mu_p^{\mathbf{K}}$, the eigenvalues of $\mathbf{K}\mathbf{R}\mathbf{K}^H$, where \mathbf{K} is a matrix such that $\mathbf{K}\mathbf{R}_0\mathbf{K} = \mathbf{I}_p$. For example, the independence test and the maximum eigenvalue test assume the forms

$$T_{\text{w-ind}} = \prod_{i=1}^p \frac{\mu_i^{\mathbf{K}} \mathcal{H}_0}{\mathcal{H}_1} \geq \xi \quad (22)$$

and

$$T_{\text{w-max}} = \mu_1^{\mathbf{K}} \frac{\mathcal{H}_0}{\mathcal{H}_1} \geq \xi \quad (23)$$

respectively.

5 Case Study: Low-cost SDR Receiver

In this section, we analyze samples collected under \mathcal{H}_0 by the RTL-SDR dongle NESDR-mini [45]. Such SDR receiver is composed by a Rafael Micro R820T tuner, an analog front-end which includes a low-noise amplifier (with controllable gain via software), RF filtering and downconversion at an intermediate frequency of 3.57 MHz. The following RTL2832U chip performs an 8 bits analog-to-digital conversion, quadrature demodulation, and sample rate reduction through decimation [46, 47]. The final sampling rate, f_s , is adjustable and can be up to 2.8 MS/s. I-Q samples are then available on the USB port [11, 48–50].

⁵Some papers, such as [23], propose to use eigenvalue-based tests also in the presence of colored noise, i.e., when the covariance matrix eigenvalues under \mathcal{H}_0 are not all equal. In this case, the decision regions of the detector and their relative position may depend on the SNR and the degree of correlation between noise samples.

<i>test</i>	<i>real part</i>	<i>imaginary part</i>
Jarque-Bera (Univariate Gaussianity)	0.953	0.952
Anderson-Darling (Univariate Gaussianity)	0.965	0.966
Henze-Zirkler (Multivariate Gaussianity)	0.941	0.942
Andersson-Perlman (Circularity)	0.999	

Table 1 Occurrence rate of Gaussianity tests for I-Q samples captured with a RTL-SDR receiver. Univariate tests are based on the observation of 1000 samples, while multivariate tests consider 4×400 matrices. Each test is performed 50000 times with a significance level of 0.05.

This low-cost device is characterized by the presence of imperfections, such as non-flat noise PSD, noise power fluctuations, and spurs caused by harmonics from the mixer, local oscillator leakage and DC offset [33, 51]. This last impairment has not been taken into consideration, assuming that spectrum sensing is preceded by spurious removal, through, e.g., an upstream spur detection and spur censoring stage [33].

5.1 Received signal characterization under \mathcal{H}_0

To validate the noise model described in Section 2, we adopt standard statistical Gaussianity tests. Table 1 shows the occurrence rate relative to 50000 tests on captured noise-only samples. All tests are performed with a significance level of 0.05. As univariate tests, we consider the Jarque-Bera and the Anderson-Darling tests, which can be adopted when the mean value and variance are not known [52–54]. Each test is performed on 1000 samples. We also considered a multivariate test, that fits the case in which samples are collected in matrices like (4). We chose, in particular, the Henze-Zirkler test proposed in [55], which has an excellent overall power against alternatives to normality [56]. All the tests show that the captured samples well fit Gaussian distributions, with about 0.95 probability. Beyond normality, we also tested the circularity property of the samples using the Andersson-Perlman test [57, 58]. These results validate the use of the Gaussian model for the received samples under \mathcal{H}_0 .

5.2 Calibration

Regarding the *whiteness* assumption, we estimated the PSD in the absence of an input signal. Except for a multiplying constant (i.e., a vertical shift in dB scale), the characteristic shape of the noise PSD is shown in Fig. 1. The multiplying constant is due to the noise power fluctuation, which causes noise power uncertainty, while the shape can be ascribed to the digital filter in the decimation stage of the RTL-SDR receiver chain [21–23]. Based on this analysis, we model noise as a Gaussian

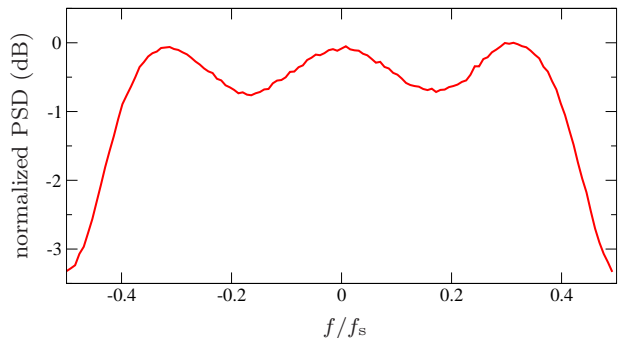


Fig. 1 Example of a spurious-free noise PSD shape measured in an RTL-SDR dongle. This normalized PSD has been estimated from samples, under \mathcal{H}_0 hypothesis, using Bartlett’s periodogram with $N_{\text{fft}} = 128$ and $N_{\text{avg}} = 1000$.

process with correlated samples, as described in Section 2.

We assume, therefore, that detection is preceded by an off-line calibration stage in which the system estimates the noise power PSD (3), for frequency-domain detectors, or the noise covariance matrix, Σ_0 , for time-domain detectors. This can be done, e.g., replacing the antenna with a $50 \, \Omega$ load. According to the noise model in Section 2, the estimated noise PSD, and the SCM are known except for a multiplicative constant related to the time-varying noise power.

The accuracy of the estimates performed in the calibration phase typically depends on its duration. A thorough analysis of such a duration is out of the scope of the paper, and it is the subject of future research. As a rule of thumb, the calibration should last at least an order of magnitude more than the detection phase.⁶

6 Numerical Results and Discussion

6.1 White noise

The performance of the detectors presented in Section 3 have been assessed by numerical simulation considering

⁶See, for example, [19], in which the length of the noise power estimation phase must be longer than the detection phase, to guarantee that the target P_{FA} and P_{D} is reached.

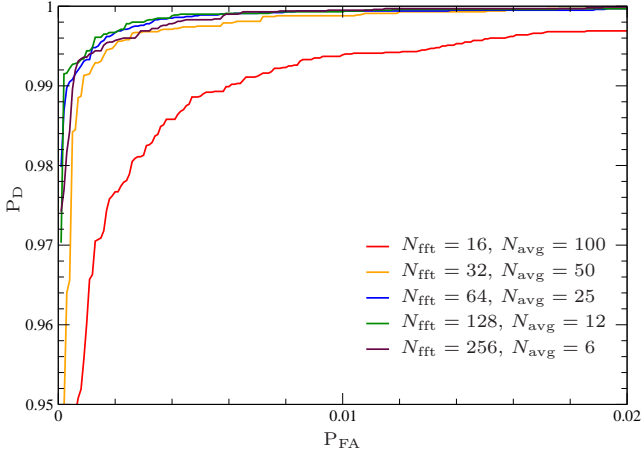


Fig. 2 ROCs for $T_{\text{enn-ed}}$, varying N_{fft} and N_{avg} with $N = 1600$, $\text{OSF} = 4$, $\text{SNR} = -10$ dB.

an orthogonal frequency-division multiplexing (OFDM) signal embedded in AWGN with $\text{SNR} = -10$ dB. The bandwidth of the OFDM signal equals $f_s/4$, i.e., $\text{OSF} = 4$.

6.1.1 Parameters setting

The performance of frequency-domain detectors introduced in Section 3.1 depends on the total number of samples collected N . Setting N , it is possible to trade-off between N_{fft} and N_{avg} for the estimation of the PSD in (2). In particular, in the following, we set $N = 1600$, and we vary N_{fft} and N_{avg} pairs such that $N_{\text{avg}} = \lfloor N/N_{\text{fft}} \rfloor$.

Fig. 2 shows the ROCs for $T_{\text{enn-ed}}$ for different N_{fft} , N_{avg} pairs. The parameter N_{fft} impacts the frequency resolution of the PSD estimate. A small N_{fft} implies, indeed, to have just a few DFT elements, each of which collects a large contribution from sidelobes. Therefore, increasing N_{fft} provides a better estimate of the in-band signal energy. Considering N_{avg} , note that it corresponds to the number of periodograms averaged in (2) and thus it impacts the accuracy of the PSD estimate. Therefore, there is a trade-off between these two parameters that provide the best performance. From Fig. 2 we can see that the best choice is $N_{\text{fft}} = 128$ and $N_{\text{avg}} = 12$. Note that increasing N_{fft} above this level, the detector performance decreases due to the small number of averages N_{avg} .⁷

Fig. 3 shows the ROCs for the frequency-domain detectors $T_{\text{f-agm}}$ and T_{sf} for different N_{fft} , N_{avg} pairs. Numerical results reveal that the best performance is obtained with $N_{\text{fft}} = 16$. This suggests that for this kind of detectors having a better PSD estimate, which

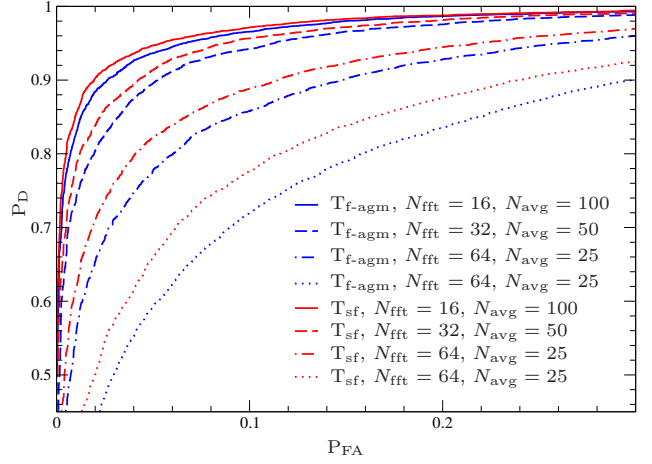


Fig. 3 ROCs for $T_{\text{f-agm}}$ and T_{sf} , varying N_{fft} and N_{avg} with $N = 1600$.

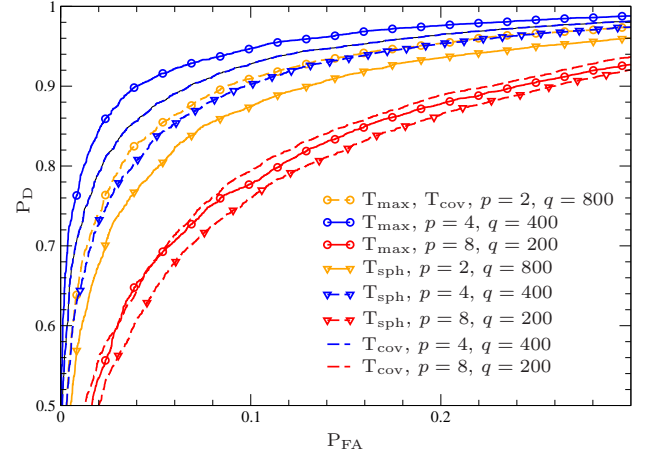


Fig. 4 ROCs for T_{max} , T_{sph} , and T_{cov} , varying p and q with $N = pq = 1600$.

can be obtained with a higher N_{avg} , is preferable than increasing the frequency resolution.

The parameter setting for the eigenvalue-based detectors is analyzed in Fig. 4. We can see that the best performance is obtained with $p = 4$, which equals OSF .

6.1.2 Detection performance comparison

Fig. 5 shows the comparison between the eigenvalue-based tests described in Section 3.2. The best performance is reached by the test T_{max} .

The general comparison between all the detectors proposed for the white noise case is presented in Fig. 6. The test $T_{\text{enn-ed}}$ provides the best detection performance considering both frequency-domain and time-domain tests. The comparison also include the autocorrelation detectors defined in Section 3.2.2. We can see that $T_{\text{ac-1}}$ outperforms T_{ac} and both provide a good detection performance when $\text{SNR}_{\text{ref}} = \text{SNR} = -10$ dB, outperforming all other detectors except for the $T_{\text{enn-ed}}$.

⁷We remark that the optimal value of N_{avg} and N_{fft} depends on the specific setting and system parameters.

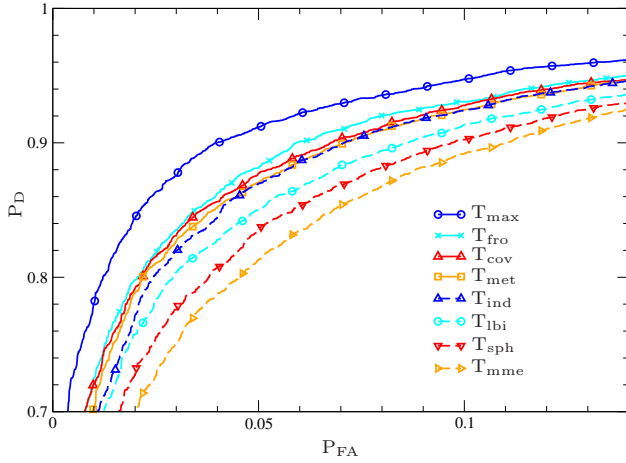


Fig. 5 ROCs for the eigenvalue-based test defined in Section 3.2, with $p = 4$ and $q = 400$.

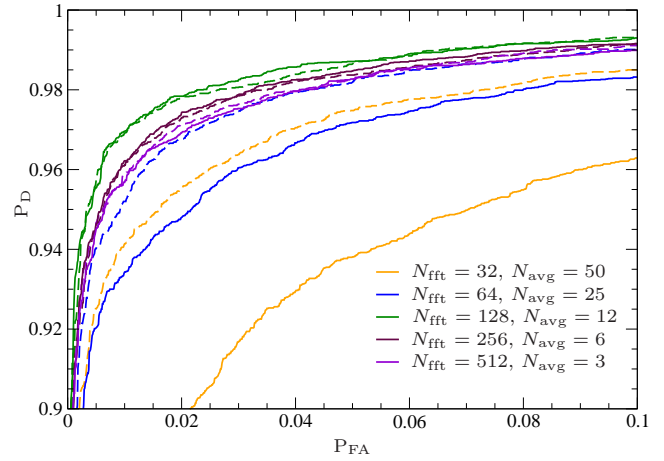


Fig. 7 ROCs for $T_{\text{enp-ed}}$ (continuous lines) and $T_{\text{w-enp-ed}}$ (dashed lines), varying N_{fft} and N_{avg} with $N = 1600$. Test on real samples captured with RTL-SDR.

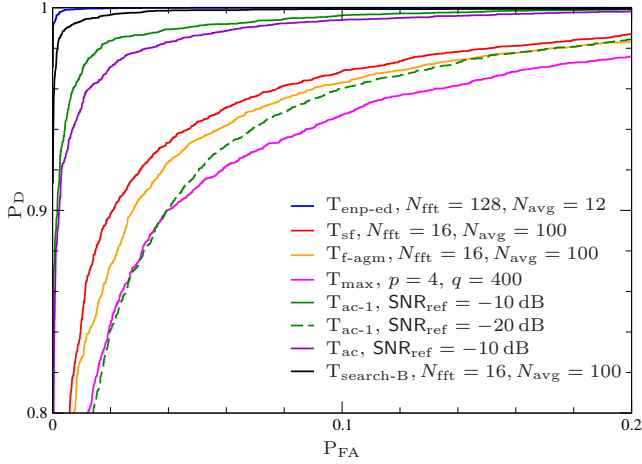


Fig. 6 ROCs for frequency-domain test and time-domain detectors in the white noise scenario, varying N_{fft} and N_{avg} , with $N = 1600$, $\text{OSF} = 4$, and $\text{SNR} = -10$ dB.

However, SNR is not known a priori in general, and considering a worst case approach, as proposed in [35], the detection performance decreases substantially. See, e.g., the case $\text{SNR}_{\text{ref}} = -20$ dB. Fig. 6 also reports the comparison between the flatness-based detectors defined in Section 3.1.2 and T_{max} , which is the best among the eigenvalue-based tests. Note that both T_{sf} and $T_{\text{f-agm}}$ outperform T_{max} . From the analysis above we can see that in general, $T_{\text{enp-ed}}$ is the best detector in the presence of oversampling. When the bandwidth and the carrier frequency of the StD are unknown, the flatness-based detectors, and in particular our proposed T_{sf} , provide a higher P_D with respect to time-domain detectors.

6.2 Colored noise

We now present the ROC curves of the detectors described in Section 4, using samples captured from the RTL-SDR dongle. The RTL-SDR receiver is tuned at 430 MHz with sampling frequency $f_s = 1$ MS/s. This frequency band has been chosen for being a signal-free band in our laboratory at the Cesena campus of the University of Bologna. The StD is an OFDM waveform transmitting independent symbols and having a 250 kHz bandwidth, generated using a USRP platform. The transmitter has been located in a non-line-of-sight position, and its transmit power has been tuned to have a SNR at the receiver equal to -10 dB.

6.2.1 Parameters setting

In this section, we analyze the trade-off between the parameters N_{fft} and N_{avg} for the frequency-based detectors described in Section 4.1.

Fig. 7 shows the ROCs for $T_{\text{enp-ed}}$ and $T_{\text{w-enp-ed}}$, for different N_{fft} , N_{avg} pairs. From Fig. 7 we can see that also in this case we have a trade-off between N_{fft} and N_{avg} , and as in the white noise case the best choice is $N_{\text{fft}} = 128$ and $N_{\text{avg}} = 12$. Regarding the comparison between the whitened and non-whitened ED, the plots confirm the advantage introduced by frequency-domain whitening, except for the cases where near-optimal values of N_{fft} and N_{avg} are chosen. In these cases, whitening does not provide substantial improvements.

In Fig. 8, the ROCs for T_{fc} , $T_{\text{wf-agm}}$, and T_{fkl} , are reported for different combinations of N_{fft} and N_{avg} , respectively. From the comparison, we can see that decreasing N_{fft} provides a higher probability of detection.

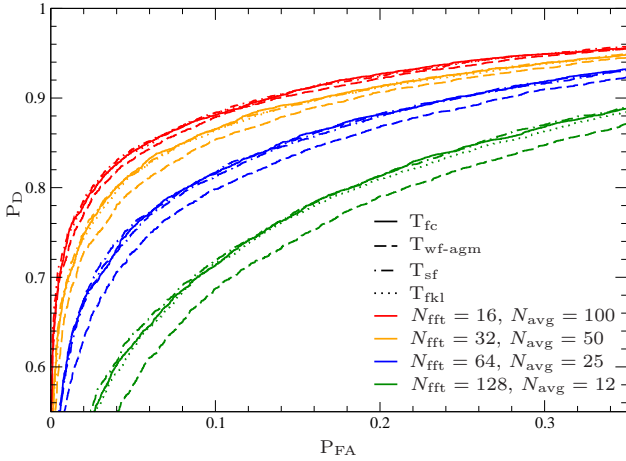


Fig. 8 ROCs for the frequency-based detectors T_{fc} (continuous), T_{wf-agm} (dashed), T_{sf} (dash-dotted), and T_{fkl} (dotted). Test on real samples captured with RTL-SDR.

6.2.2 Detection performance comparison

Fig. 9 shows a comparison between the ROCs of the frequency-based detectors of Section 4.1 and the time-domain tests described in Section 4.2. We adopt, in this case, the parameters N_{fft} and N_{avg} that maximize the detection performance for each test. For the eigenvalue-based detectors we adopt $p = OSF = 4$. From the comparison, we can see that frequency-domain detectors outperform eigenvalue-based tests. Note, in particular, that T_{enp-ed} provides the best performance with much higher detection probability compared to other detectors. For example, when $P_{FA} = 0.01$ the probability of detection of T_{enp-ed} is approximately $P_D = 0.97$, while for T_{fc} is $P_D = 0.74$ and for T_{w-max} is $P_D = 0.65$.

The significant detection performance gain of the ENP-ED can be explained because T_{enp-ed} exploits additional information with respect to other detectors. Note, indeed, that T_{enp-ed} requires the knowledge of the signal band, \mathcal{B} . This is a valid assumption, for example, when the signal to be detected is a PU, whose channelization is generally known from standards and regulations.

In different CR scenarios, however, \mathcal{B} is unknown, and the best choice is to adopt T_{fc} , which does not require any knowledge of the signal to be detected (including its operating band) and that provides better detection performance than T_{wf-agm} and eigenvalue-based tests.

7 Conclusion

In this paper, we discussed the problem of WSS in the presence of oversampling, i.e., when the sampling frequency is larger than the signal bandwidth. We consid-

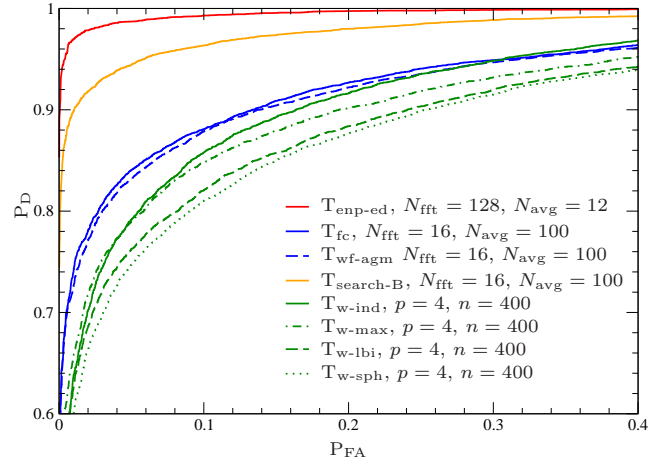


Fig. 9 ROC comparison of frequency-domain tests and time-domain detectors. Samples captured with RTL-SDR.

ered both the white noise case, which fits well-designed receivers, and the colored noise case, which fits inexpensive devices in which front-end non-idealities cannot be neglected. Considering the latter case, we studied the receiver characteristic of a low-cost commercial device. We analyzed several detectors, proposing some frequency-domain tests which have been demonstrated to outperform time-domain approaches, such as the standard eigenvalue-based tests. The analysis showed that the best detection performance is provided by a noise-uncertainty immune ED and, for the colored noise case, by tests that match the PSD of the receiver noise.

Appendix

The ENP-ED detector (8) can be derived as a GLRT assuming AWGN and a signal described as a white Gaussian process with bandwidth B . Let us organize \mathbf{y} as a sequence of N_{avg} vectors \mathbf{y}_k of length N_{fft} with $k = 1, \dots, N_{avg}$, and let $\tilde{\mathbf{y}}_k$ be the DFT of \mathbf{y}_k . Under the hypotheses made, the spectral representation $\tilde{\mathbf{y}}_k$ is Gaussian distributed with covariance $\tilde{\Sigma}_j$ with $j = 0, 1$, depending on the presence/absence of the StD. Under \mathcal{H}_0 its covariance matrix is $\tilde{\Sigma}_0 = \sigma^2 \mathbf{I}_{N_{fft}}$, while under \mathcal{H}_1 the covariance $\tilde{\Sigma}_1$ is a diagonal matrix in which the elements within the signal band are all equal to $\sigma_t^2 = \sigma_s^2 + \sigma^2$, and the others equal to σ^2 . Thus the joint distribution of the vectors $\tilde{\mathbf{y}}_k$ is given by

$$f(\{\tilde{\mathbf{y}}_k\}_{k=1}^{N_{avg}} | \mathcal{H}_j) = \frac{1}{\pi^{N_{fft} N_{avg}} |\tilde{\Sigma}_j|^{N_{avg}}} \times \exp\left(-\sum_k \tilde{\mathbf{y}}_k^H \tilde{\Sigma}_j^{-1} \tilde{\mathbf{y}}_k\right).$$

The likelihood ratio (LR) of $\tilde{\mathbf{y}}_k$ is therefore

$$\begin{aligned}\mathcal{L} &= f(\{\tilde{\mathbf{y}}_k\}_{k=1}^{N_{\text{avg}}} | \mathcal{H}_1) / f(\{\tilde{\mathbf{y}}_k\}_{k=1}^{N_{\text{avg}}} | \mathcal{H}_0) \\ &= \frac{|\tilde{\mathbf{\Sigma}}_0|}{|\tilde{\mathbf{\Sigma}}_1|} e^{N_{\text{fft}} \text{tr}\{\tilde{\mathbf{\Sigma}}_0^{-1} \tilde{\mathbf{S}}\} - N_{\text{fft}} \text{tr}\{\tilde{\mathbf{\Sigma}}_1^{-1} \tilde{\mathbf{S}}\}} \\ &= \frac{(\sigma^2)^{N_{\text{fft}} N_{\text{avg}}}}{(\sigma^2)^{(N_{\text{fft}} - |\mathcal{S}|) N_{\text{avg}}} (\sigma_t^2)^{|\mathcal{S}| N_{\text{avg}}}} e^{N_{\text{fft}} ((\sigma^2)^{-1} \text{tr}\{\tilde{\mathbf{S}}\})} \\ &\quad \times e^{-N_{\text{fft}} ((\sigma_t^2)^{-1} \sum_{i \in \mathcal{S}} \tilde{s}_{i,i} + (\sigma^2)^{-1} \sum_{i \in \bar{\mathcal{S}}} \tilde{s}_{i,i})} \quad (24)\end{aligned}$$

where \mathcal{S} is the set of the indexes of the frequency bins within the signal band, $|\mathcal{S}|$ is its cardinality and the SCM is given by $\tilde{\mathbf{S}} = \sum_{k=1}^{N_{\text{avg}}} \tilde{\mathbf{y}}_k \tilde{\mathbf{y}}_k^H / N_{\text{avg}}$. Under \mathcal{H}_0 , the maximum likelihood (ML) estimate of σ^2 is $\hat{\sigma}_{\mathcal{H}_0}^2 = \sum_i s_{i,i} / N_{\text{fft}}$, while under \mathcal{H}_1 we get $\hat{\sigma}_{\mathcal{H}_1}^2 = \sum_{i \in \mathcal{S}} \tilde{s}_{i,i} / |\mathcal{S}|$ and $\hat{\sigma}_{\mathcal{H}_0}^2 = \sum_{i \in \bar{\mathcal{S}}} \tilde{s}_{i,i} / (N_{\text{fft}} - |\mathcal{S}|)$. Substituting the estimates into (24) we obtain

$$\mathcal{L} = \kappa \left(1 + \frac{\sum_{i \in \mathcal{S}} \tilde{s}_{i,i}}{\sum_{i \in \bar{\mathcal{S}}} \tilde{s}_{i,i}} \right)^{N_{\text{fft}} N_{\text{avg}}} \left(\frac{\sum_{i \in \mathcal{S}} \tilde{s}_{i,i}}{\sum_{i \in \bar{\mathcal{S}}} \tilde{s}_{i,i}} \right)^{-|\mathcal{S}| N_{\text{avg}}} \quad (25)$$

where the constant κ contains terms that do not depend on the signal samples. Finally, from (25) we get the sufficient statistic

$$\frac{\sum_{i \in \mathcal{S}} \tilde{s}_{i,i}}{\sum_{i \in \bar{\mathcal{S}}} \tilde{s}_{i,i}} = \frac{\|\mathbf{p}[\mathcal{S}]\|_1}{\|\mathbf{p}[\bar{\mathcal{S}}]\|_1} \quad (26)$$

which corresponds to the ENP-ED test $T_{\text{enp-ed}}$ in (8).

References

1. National Spectrum Consortium. [Online]. Available: <https://www.nationalspectrumconsortium.org>
2. M. Chiani, A. Giorgetti, and E. Paolini, "Sensor radar for object tracking," *Proc. IEEE*, vol. 106, no. 6, pp. 1022–1041, Jun. 2018.
3. S. Kandeepan and A. Giorgetti, *Cognitive Radios and Enabling Techniques*. Boston, USA: Artech House Publishers, Nov. 2012.
4. A. Sharma, A. Mariani, A. Giorgetti, D. Mitra, and M. Chiani, "Subspace-based spectrum guarding," in *Proc. IEEE Int. Conf. on Commun. (ICC 2015)*, London, UK, Jun. 2015.
5. J. Mitola, "Software radios: Survey, critical evaluation and future directions," *IEEE Aerosp. Electron. Syst. Mag.*, vol. 8, no. 4, pp. 25–36, Apr. 1993.
6. E. Buracchini, "The software radio concept," *IEEE Commun. Mag.*, vol. 38, no. 9, pp. 138–143, Sep. 2000.
7. F. K. Jondral, "Software-defined radio: basics and evolution to cognitive radio," *EURASIP journal on wireless communications and networking*, vol. 2005, no. 3, pp. 275–283, Aug. 2005.
8. A. M. Wyglinski, D. P. Orofino, M. N. Ettus, and T. W. Rondeau, "Revolutionizing software defined radio: Case studies in hardware, software, and education," *IEEE Commun. Mag.*, pp. 68–75, Jan. 2016.
9. R. Bagheri, A. Mirzaei, M. E. Heidari, S. Chehrizi, M. Lee, M. Mikhemar, W. K. Tang, and A. A. Abidi, "Software-defined radio receiver: dream to reality," *IEEE Commun. Mag.*, vol. 44, no. 8, pp. 111–118, Aug. 2006.
10. A. A. Abidi, "The path to the software-defined radio receiver," *IEEE J. Solid-State Circuits*, vol. 42, no. 5, pp. 954–966, May 2007.
11. R. W. Stewart, K. W. Barlee, D. S. W. Atkinson, and L. H. Crockett, *Software Defined Radio using MATLAB & Simulink and the RTL-SDR*, 1st ed. Glasgow, Scotlabd, UK: Wiley, 2015.
12. Ettus Research. Universal Software Radio Peripheral. [Online]. Available: <https://www.ettus.com/product>
13. A. Mariani, S. Kandeepan, and A. Giorgetti, "Periodic spectrum sensing with non-continuous primary user transmissions," *IEEE Trans. Wireless Commun.*, vol. 14, no. 3, pp. 1636–1649, Mar. 2015.
14. A. Mariani, A. Giorgetti, and M. Chiani, "Wideband spectrum sensing by model order selection," *IEEE Trans. Wireless Commun.*, vol. 14, no. 12, pp. 6710–6721, Dec. 2015.
15. E. H. Gismalla and E. Alsusa, "On the performance of energy detection using bartlett's estimate for spectrum sensing in cognitive radio systems," *IEEE Trans. on Signal Proc.*, vol. 60, no. 7, pp. 3394–3404, July 2012.
16. J. Verlant-Chenet, J. Renard, J. M. Dricot, P. D. Doncker, and F. Horlin, "Sensitivity of spectrum sensing techniques to RF impairments," in *2010 IEEE 71st Vehicular Technology Conference*, May 2010, pp. 1–5.
17. A. Zahedi-Ghasabeh, A. Tarighat, and B. Daneshrad, "Cyclo-stationary sensing of OFDM waveforms in the presence of receiver RF impairments," in *IEEE Wireless Comm. and Netw. Conf.*, April 2010, pp. 1–6.
18. J. G. Proakis, *Digital communications*, 4th ed. New York: McGraw-Hill, 2001.
19. A. Mariani, A. Giorgetti, and M. Chiani, "Effects of noise power estimation on energy detection for cognitive radio applications," *IEEE Trans. Commun.*, vol. 59, no. 12, pp. 3410–3420, Dec. 2011.
20. L. Wei, O. Tirkkonen, and Y.-C. Liang, "Multi-source signal detection with arbitrary noise covariance," *IEEE Trans. Signal Process.*, vol. 62, no. 22, pp. 5907–5918, Nov. 2014.
21. Y. Zeng and Y.-C. Liang, "Eigenvalue-based spectrum sensing algorithms for cognitive radio," *IEEE Trans. Commun.*, vol. 57, no. 6, pp. 1784–1793, Jun. 2009.
22. R. N. McDonough and A. Whalen, *Detection of signals in noise*. Academic Press, 1995.
23. S. K. Sharma, S. Chatzinotas, and B. Ottersten, "Eigenvalue-based sensing and SNR estimation for cognitive radio in presence of noise correlation," *IEEE Trans. Veh. Technol.*, vol. 62, no. 8, pp. 3671–3684, Oct. 2013.
24. A. Sonnenschein and P. M. Fishman, "Radiometric detection of spread-spectrum signals in noise of uncertain power," *IEEE Trans. Aerosp. Electron. Syst.*, vol. 28, no. 3, pp. 654–660, Jul. 1992.
25. D. Torrieri, "The radiometer and its practical implementation," in *Proc. IEEE Military Commun. Conf. (MILCOM 2010)*, Oct./Nov. 2010, pp. 304–310.
26. A. Mariani, A. Giorgetti, and M. Chiani, "Wideband spectrum sensing by model order selection," *IEEE Trans. Wireless Commun.*, vol. 14, no. 12, pp. 6710–6721, Dec. 2015.
27. —, "Test of independence for cooperative spectrum sensing with uncalibrated receivers," in *Proc. IEEE Global Commun. Conf. (GLOBECOM 2012)*, Anaheim, CA, USA, Dec. 2012.

28. —, “Recent advances on wideband spectrum sensing for cognitive radio,” in *Cognitive Communications and Cooperative HetNet Coexistence, Signals and Communication Technology* (M.-G. Di Benedetto and F. Bader, Eds.). Switzerland: Springer Int. Pub., 2014, ch. 1.
29. F. Penna, R. Garello et al., “Cooperative spectrum sensing based on the limiting eigenvalue ratio distribution in wishart matrices,” *IEEE Commun. Lett.*, vol. 13, no. 7, pp. 507–509, Jul. 2009.
30. A. Mariani, A. Giorgetti, and M. Chiani, “Designing ITC selection algorithms for wireless sources enumeration,” in *IEEE Int. Conf. on Comm. (ICC 2015)*, London, UK, Jun. 2015, pp. 4883–4888.
31. A. H. Gray Jr and J. D. Markel, “A spectral-flatness measure for studying the autocorrelation method of linear prediction of speech analysis,” *IEEE Trans. Acoust., Speech, Signal Process.*, vol. 22, no. 3, pp. 207–217, Jun. 1974.
32. A. Mariani, A. Giorgetti, and M. Chiani, “Model order selection based on information theoretic criteria: Design of the penalty,” *IEEE Trans. Signal Process.*, vol. 63, no. 11, pp. 2779–2789, Jun. 2015.
33. H. Cao and J. Peissig, “Practical spectrum sensing with frequency-domain processing in cognitive radio,” in *Proc. European Signal Process. Conf. (EUSIPCO 2012)*, Bucharest, Romania, Aug. 2012, pp. 435–439.
34. G. B. Giannakis and C. Tepedelenlioglu, “Basis expansion models and diversity techniques for blind identification and equalization of time-varying channels,” *Proc. IEEE*, vol. 86, no. 10, pp. 1969–1986, 1998.
35. W. Han, C. Huang, J. Li, Z. Li, and S. Cui, “Correlation based spectrum sensing with over-sampling in cognitive radio,” *IEEE J. Sel. Areas Commun.*, vol. 33, no. 5, May 2015.
36. J. Lundén, S. A. Kassam, and V. Koivunen, “Robust nonparametric cyclic correlation-based spectrum sensing for cognitive radio,” *IEEE Trans. Signal Process.*, vol. 58, no. 1, pp. 38–52, Aug. 2010.
37. J. G. Proakis and D. G. Manolakis, *Digital Signal Processing: Principles, Algorithms, and Applications*, 3rd ed. Prentice Hall, 1996.
38. J. Mauchly, “Significance test for sphericity of a normal n-variate distribution,” *The Annals of Mathematical Statistics*, vol. 11, no. 2, pp. 204–209, Jun. 1940.
39. S. John, “Some optimal multivariate tests,” *Biometrika*, vol. 58, no. 1, pp. 123–127, Apr. 1971.
40. A. Leshem and A.-J. van der Veen, “Multichannel detection of Gaussian signals with uncalibrated receivers,” *IEEE Signal Process. Lett.*, vol. 8, no. 4, pp. 120–122, Apr. 2001.
41. Y. Zeng and Y.-C. Liang, “Spectrum-sensing algorithms for cognitive radio based on statistical covariances,” *IEEE Trans. Veh. Technol.*, vol. 58, no. 4, pp. 1804–1815, May 2009.
42. M. Naraghi-Pour and T. Ikuma, “Autocorrelation-based spectrum sensing for cognitive radios,” *IEEE Trans. Veh. Technol.*, vol. 59, no. 2, pp. 718–733, Feb. 2010.
43. M. Jin, Y. Li, and H.-G. Ryu, “On the performance of covariance based spectrum sensing for cognitive radio,” *IEEE Trans. Signal Process.*, vol. 60, no. 7, pp. 3670–3682, Jul. 2012.
44. H. So, W. Ma, and Y. Chan, “Detection of random signals via spectrum matching,” *IEEE Trans. Aerosp. Electron. Syst.*, vol. 38, no. 1, pp. 301–307, Jan. 2002.
45. NooElec Inc. NESDR Mini SDR and DVB-T USB Stick (RTL2832U + R820T). [Online]. Available: <http://www.nooelec.com/>
46. T. Hentschel, M. Henker, and G. Fettweis, “The digital front-end of software radio terminals,” *IEEE Personal Commun.*, vol. 6, no. 4, pp. 40–46, Aug. 1999.
47. G. Sklivanitis, A. Gannon, S. N. Batalama, and D. A. Pados, “Addressing next-generation wireless challenges with commercial software-defined radio platforms,” *IEEE Commun. Mag.*, pp. 59–67, Jan. 2016.
48. Realtek, Taiwan. (2012, Dec.) Realtek rtl2832u. [Online]. Available: <http://www.realtek.com.tw/products/>
49. O. Guillán-Lorenzo and F. J. Díaz-Otero, “Diseño de un receptor basado en rtl2832u para la medida del contenido electrónico de la ionosfera,” in *Proc. XXVIII Simposium nacional del la unión científica internacional de radio (URSI 2013)*, Santiago de Compostela, Spain, Sep. 2013.
50. R. K. Kodali, L. Boppana, and S. R. Kondapalli, “DDC and DUC Filters in SDR platforms,” in *Proc. IEEE Int. Conf. on Advanced Computing Technol. (ICACT 2013)*, Sep. 2013.
51. D. Borio, E. Angiuli, R. Giuliani, and G. Baldini, “Robust spectrum sensing demonstration using a low-cost front-end receiver,” *Int. J. Antenn. Propag.*, 2015.
52. B. Yazici and S. Yolacan, “A comparison of various tests of normality,” *Journal of Statistical Computation and Simulation*, vol. 77, no. 2, pp. 175–183, Feb. 2007.
53. M. A. Stephens, “EDF statistics for goodness of fit and some comparisons,” *Journal of the American Statistical Association*, vol. 69, no. 347, pp. 730–737, Sep. 1974.
54. N. M. Razali and Y. B. Wah, “Power comparisons of Shapiro-Wilk, Kolmogorov-Smirnov, Lilliefors and Anderson-Darling tests,” *Journal of Statistical Modeling and Analytics*, vol. 2, no. 1, pp. 21–33, 2011.
55. N. Henze and B. Zirkler, “A class of invariant consistent tests for multivariate normality,” *Communications in Statistics-Theory and Methods*, vol. 19, no. 10, pp. 3595–3617, 1990.
56. C. J. Mecklin and D. J. Mundfrom, “On using asymptotic critical values in testing for multivariate normality,” *InterStat*, vol. 1, no. 1-12, p. 152, 2003.
57. S. A. Andersson and M. D. Perlman, “Two testing problems relating the real and complex multivariate normal distributions,” *Journal of Multivariate Analysis*, vol. 15, no. 1, pp. 21–51, 1984.
58. T. Adali, P. J. Schreier, and L. L. Scharf, “Complex-valued signal processing: The proper way to deal with impropriety,” *IEEE Trans. Signal Process.*, vol. 59, no. 11, pp. 5101–5125, Nov. 2011.



Andrea Mariani received the B.Sc. degree in Biomedical Engineering (with honors) in 2006, the M.Sc. degree in Electronics and Telecommunications Engineering (with honors) in 2009, and the Ph.D. degree in Electronics, Computer Science and Telecommunications in 2013 from the University of Bologna, Italy. From 2013 to 2016, he was with the Center for Industrial Research on ICT (CIRI-ICT) of the University of Bologna. In 2016 he joined Onit Group, Italy, as R&D Manager for the Industry Division. He has participated in several international projects, such as FP7-ICT EUWB, FP7-ICT SELECT and EDA-B CORASMA projects.

His research interests include statistical signal processing and digital communications, with particular emphasis on localization, spectrum sensing for cognitive radio networks and software defined radio.

Dr. Mariani was a member of the Technical Program Committee of the Cognitive Radio and Networks Symposium at the IEEE Int. Conf. on Commun. (ICC 2013 - 2016), the Cognitive Radio and Networks Symposium at the IEEE Global Commun. Conf. (Globecom 2013), and was a member of the local organization committee for the IEEE Int. Conf. on Ultra-WideBand (ICUWB 2011). He serves as reviewer for several IEEE Journals and Conferences, and has been named an Exemplary Reviewer for the IEEE WIRELESS COMMUNICATIONS LETTERS in 2013 and for the IEEE COMMUNICATIONS LETTERS in 2013 and 2014.

Andrea Giorgetti received the Dr. Ing. degree (*summa cum laude*) in electronic engineering and the Ph.D. degree in electronic engineering and computer science from the University of Bologna, Italy, in 1999 and 2003, respectively. From 2003 to 2005, he was a Researcher with the National Research Council, Italy. He joined the Department of Electrical, Electronic, and Information Engineering “Guglielmo Marconi,” University of Bologna, as an Assistant Professor in 2006 and was promoted to Associate Professor



in 2014. In spring 2006, he was with the Laboratory for Information and Decision Systems (LIDS), Massachusetts Institute of Technology (MIT), Cambridge, MA, USA. Since then, he has been a frequent visitor to the Wireless Information and Network Sciences Laboratory at the MIT, where he presently holds the Research Affiliate appointment.

His research interests include ultrawide bandwidth communication systems, active and passive localization, wireless sensor networks, and cognitive radio. He has co-authored the book *Cognitive Radio Techniques: Spectrum Sensing, Interfer-*

ence Mitigation, and Localization (Artech House, 2012). He was the Technical Program Co-Chair of several symposia at the IEEE Int. Conf. on Commun. (ICC), and IEEE Global Commun. Conf. (Globecom). He has been an Editor for the IEEE COMMUNICATIONS LETTERS and for the IEEE TRANSACTIONS ON WIRELESS COMMUNICATIONS. He has been elected Chair of the IEEE Communications Society’s Radio Communications Technical Committee.



Marco Chiani received the Dr. Ing. degree (*summa cum laude*) in electronic engineering and the Ph.D. degree in electronic and computer engineering from the University of Bologna, Italy, in 1989 and 1993, respectively.

He is a Full Professor in Telecommunications at the University of Bologna. During summer 2001, he was a Visiting Scientist at AT&T Research Laboratories, Middletown, NJ. Since 2003 he has been a frequent visitor at the Massachusetts Institute of Technology (MIT), Cambridge, where he

presently holds a Research Affiliate appointment. His research interests are in the areas of communications theory, wireless systems, and statistical signal processing, including MIMO statistical analysis, codes on graphs, wireless multimedia, cognitive radio techniques, and ultra-wideband radios.

In 2012 he has been appointed Distinguished Visiting Fellow of the Royal Academy of Engineering, UK. He is the past chair (2002–2004) of the Radio Communications Committee of the IEEE Communication Society and past Editor of Wireless Communication (2000–2007) for the journal IEEE TRANSACTIONS ON COMMUNICATIONS. He received the 2011 IEEE Communications Society Leonard G. Abraham Prize in the Field of Communications Systems, the 2012 IEEE Communications Society Fred W. Ellersick Prize, and the 2012 IEEE Communications Society Stephen O. Rice Prize in the Field of Communications Theory.